九州工業大学学術機関リポジトリ

**Kyutacar**

Kyushu Institute of Technology Academic Repository

# Development of hafnium metal and titanium-hafnium alloys having apatite-forming ability by chemical surface modification

# Development of hafnium metal and titanium-hafnium alloys having apatite-forming ability by chemical surface modification

**Development of hafnium metal and titanium-hafnium alloys having apatite-forming ability by chemical surface modification**

Toshiki Miyazaki[a],[*], Masaya Sueoka[a], Yuki Shirosaki[b], Nobuya Shinozaki[a] and Takanobu Shiraishi[c]

[a]Graduate School of Life Science and System Engineering, Kyushu Institute of Technology, Kitakyushu, Japan

[b]Graduate School of Engineering, Kyushu Institute of Technology, Kitakyushu, Japan

[c]Graduate School of Biomedical Sciences, Nagasaki University, Nagasaki, Japan

Corresponding author:

Toshiki Miyazaki

Graduate School of Life Science and Systems Engineering, Kyushu Institute of Technology, 2-4, Hibikino, Wakamatsu-ku, Kitakyushu 808-0196, Japan

Tel/Fax: +81-93-695-6025

E-mail: tmiya@life.kyutech.ac.jp

**Abstract**

Hafnium (Hf) has attracted considerable attention as a component of biomedical titanium

(Ti) alloys with low Young's moduli and/or shape-memory functionalities, because its

cytotoxicity is as low as that of Ti. The drawback of metals is that their bone-bonding

ability is generally low. It is known that apatite formation in the body is a prerequisite for

bone-bonding. Although several chemical treatments have been proposed for preparing

Ti for bone-bonding, there have been no similar investigations for Hf. In the present study,

NaOH- and heat-treatments were applied to pure Hf and Ti-Hf alloys and their

bone-bonding ability was assessed *in vitro* with the use of simulated body fluid (SBF).

After NaOH- and heat-treatments, anatase formed on alloys with low Hf content (20–

40% (atom%) Hf); mixtures of sodium titanate and hafnium titanate formed on alloys

with similar Ti and Hf content (60% Hf); and hafnium oxide formed on alloys with high

Hf content (80% Hf and pure Hf). Precipitates of apatite were observed on all the metals

in SBF, except for the alloy with 60% Hf. We speculated that the hafnium titanate formed

on this alloy had a low apatite-forming ability owing to its high negative surface charge,

which inhibited P adsorption. The apatite-forming abilities of the Ti-Hf alloys strongly

depended on their Hf content. The present results indicate that Hf-based materials have

good potential for bone-bonding.

**Keywords:** Hafnium, Titanium-hafnium alloy, Bone-bonding, Surface treatment,

Apatite

## 1. Introduction

Hafnium (Hf) belongs to the same group of elements as titanium (Ti) and zirconium (Zr), which are applied for clinical replacement of hard tissue and have similar chemical properties. It is known that the cytotoxicity of hafnium is as low as that of Ti and Zr [1]. Recently, addition of Hf to Ti has been found to reduce the Young's modulus of the resulting alloy from 120 to 110 GPa [2,3]. In addition, Hf has attracted considerable attention as a component of nickel-free shape memory alloys for medical applications [4].

However, many metallic materials do not bind with bone easily and this property must be improved to enable their application to hard tissue reconstruction. An essential requirement for artificial materials to exhibit bone-bonding in the body is the formation of a bone-like apatite layer [5]. Chemical treatments based on aqueous solutions of sodium hydroxide (NaOH) [6] or hydrogen peroxide [7], followed by heat treatments, and anodic oxidation [8] are known to be effective techniques for enhancing the apatite-forming ability on Ti metal surfaces. Tantalum (Ta) [9] and Zr [10] can also exhibit bone-bonding properties following NaOH treatments. However, the effects of such surface treatments on Hf remain unclear.

In this study, pure Hf metal and Ti-Hf alloys were subjected to NaOH- and

heat-treatments and the apatite-forming abilities of the treated alloys were investigated in

simulated body fluid (SBF). Differences in the apatite-forming ability are discussed in

terms of the components of the alloy and the crystalline phase of the surface after the

treatments.

## 2. Materials and methods

### 2.1. Materials

NaOH and the reagents used to prepare SBF were purchased from Nacalai Tesque

Inc., Kyoto, Japan, hafnium oxide ($HfO_2$) from Kojundo Chemical Laboratory Co., Ltd.

Saitama, Japan, and anatase from Ishihara Sangyo Kaisha, Ltd., Osaka, Japan.

### 2.2. NaOH- and heat-treatments

Pure Hf substrates (Nilaco Co., Tokyo, Japan) $10 \times 10 \times 0.1$ mm$^3$ in size and Ti-Hf

alloy substrates (Kindly prepared by arc melting in Institute for Materials Research,

Tohoku University, Sendai, Japan) $5 \times 5 \times 7$ mm$^3$ in size were polished with #500 SiC

5

paper. Ti-Hf alloy containing x atom% of Hf is hereafter denoted as Ti-xHf. Each

substrate was then soaked in 5 mL of 10 M-NaOH aqueous solution and mechanically

agitated in a water bath (H-10, Taitec Co., Saitama, Japan) at 60 °C for 1 day. The

agitating speed was fixed at 120 strokes/min. The substrates were then removed from

solution, gently washed with ultrapure water, and dried at 60°C. The substrates were

then heated to 400°C at 5 °C/min, maintained at 400°C for 1 h, and allowed to cool to

room temperature in the furnace.

Hafnium oxide and hafnium titanate (HfTiO$_4$) powders were used for zeta potential

measurements as model compounds for the surface crystal phase of the chemically

treated metals. The HfO$_2$ reagent was used as received. HfTiO$_4$ was prepared by

calcinating a mixture of HfO$_2$ and anatase at a molar ratio of 1:1 at 1300°C for 5 h.

X-ray diffraction measurements confirmed that the obtained powder consisted of a

single phase of HfTiO$_4$ (JCPDS#40-794).

2.3. Soaking in SBF

The treated substrates were soaked in 30 mL of SBF containing the following

inorganic ion concentrations (142.0 mM $Na^+$, 5.0 mM $K^+$, 1.5 mM $Mg^{2+}$, 2.5 mM $Ca^{2+}$,

147.8 mM $Cl^-$, 4.2 mM $HCO_3^-$, 1.0 mM $HPO_4^{2-}$, and 0.5 mM $SO_4^{2-}$) at 36.5 °C for

various periods. The pH of the solution was buffered at 7.40 by 50 mM

tris(hydroxymethyl)aminomethane and an appropriate amount of HCl. SBF was

prepared according to the literature [11]. After soaking, the substrates were removed

from the SBF and then immersed in ultrapure water for 30 min to remove excess

water-soluble salts on their surfaces.

2.4. Characterization

The surface structural changes of the substrates were characterized by scanning

electron microscope imaging (SEM; Model S-3500N; Hitachi Co., Tokyo, Japan),

energy dispersive X-ray spectroscopy (EDX; Model EX-400; Horiba Co., Kyoto, Japan),

thin-film X-ray diffraction (TF-XRD; MXP3V; Mac Science Ltd., Yokohama, Japan),

X-ray photoelectron spectroscopy (XPS, KRATOS AXIS-Nova, Shimadzu Co., Kyoto,

Japan) and Fourier-transform infrared spectroscopy (FT-IR, FT/IR-6100, JASCO Co.,

Tokyo, Japan). Zeta potentials of the powder in 10 mM NaCl were measured with a

7

zeta-potential analyzer (ELS-Z, Otsuka Electronics Co., Osaka, Japan) in a connected

box-like quartz cell. The obtained zeta potential was statistically analyzed by t-test.

In TF-XRD experiments, the incident beam was fixed at 1° to the surface of each

substrate, at a scan rate of $0.02°·s^{-1}$. In XPS experiments, the measured binding energies

were corrected against the C1s binding energy of hydrocarbon methylene groups (284.6

eV) adsorbed on the substrate surface. In FT-IR measurements, an attenuated total

reflection (ATR) attachment with a diamond crystal was used.

## 3. Results

Fig. 1 shows XPS spectra of NaOH- and heat-treated metal substrates. Peaks at 530 eV

are assigned to M-O (M: Ti, Hf), those at 531 eV to acidic M-OH or physically adsorbed

water, and those at 532.5 eV to basic M-OH or chemically adsorbed water [12]. The

proportion of the peak attributed to basic M-OH groups or chemically adsorbed water

increased as the Ti content in the alloy increased. This result indicates that the NaOH- and

heat-treatments induced the largest proportion of M-OH groups on the surface of the

alloys with high Ti content.

Fig. 2 shows TF-XRD patterns of the NaOH- and heat-treated metal substrates before and after immersion in SBF for 7 days. Peaks assigned to the $\alpha'$ phase of Ti-Hf with a hexagonal close-packed structure shifted to a lower diffraction angle as the Hf content in increased in the alloy. Peaks assigned to anatase (JCPDS#21-1272) were observed for Ti-20Hf and Ti-40Hf; peaks assigned to $Na_2Ti_5O_{11}$ (JCPDS#11-289) and $HfTiO_4$ (JCPDS#40-794) were found in Ti-60Hf; peaks assigned to $HfO_2$ (JCPDS#34-104) were found in Ti-80Hf and Hf. Such crystalline phase was not observed except base metal just after NaOH treatment (data not shown), meaning that the above oxides were formed by the heating. The crystalline phases remained almost the same even after immersion in SBF.

Fig. 3 shows SEM images and EDX spectra of the NaOH- and heat-treated metal substrates after immersion in SBF for 7 days. Formation of spherical particles was observed on the surfaces of the alloys except for the Ti-60Hf substrate. The particles were confirmed to contain a high proportion of Ca and P by EDX.

Fig. 4 shows a high-magnification SEM image and FT-IR ATR spectrum of the spherical particles formed on the surface-treated Ti-80Hf after immersion in SBF for 7

9

days. A fine network morphology was observed, which was similar to that of the bone-like apatite formed in SBF [13]. In the FT-IR ATR spectrum, peaks assigned to $PO_4^{3-}$, $HPO_4^{2-}$ and $CO_3^{2-}$ were observed [14,15]. The peak of $HPO_4^{2-}$ and $CO_3^{2-}$ around 870 cm$^{-1}$ was too close to distinguish from each other. The splitting of the $PO_4^{3-}$ peaks at 600 and 1000 cm$^{-1}$ is characteristic of apatite, and the presence of $CO_3^{2-}$ suggested the formation of carbonate-containing non-stoichiometric apatite in SBF [16]. Therefore, the spherical particles in Fig. 3 are considered to be bone-like apatite.

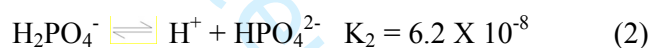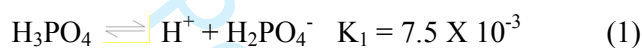Table 1 shows the zeta potentials of $HfO_2$ and $HfTiO_4$, indicating that $HfTiO_4$ had a more negative surface charge than that of $HfO_2$.

## 4. Discussion

We found that NaOH- and heat-treated Hf metal formed apatite on their surfaces in SBF. This result confirms that the Hf-OH group can act as a functional group that enables apatite formation, as previously reported for Si-OH and Ti-OH groups.

The calcium phosphate precipitates formed on the substrates could not be identified as an apatite phase by TF-XRD, likely because of the small amount present. However, it

10

has been reported that pure Ti treated with 5 M-NaOH and heated at 400°C forms

apatite over its whole surface in SBF within 7 days [17]. Therefore, we observe that the

apatite-forming ability of the Ti-Hf alloy and Hf metal is lower than that of pure Ti.

There are two possible reasons for this result: First, the apatite-forming ability of

Hf-OH itself is lower than that of Ti-OH. Second, Ti has a higher corrosion rate (5.0

mm / year in 40% NaOH at 121°C) in NaOH solution than that of Hf (0.15 mm / year in

38% NaOH at 115°C) [18,19]. Therefore, it is likely that fewer Hf-OH groups were

formed by the NaOH- and heat-treatments, in spite that we used more concentrated

NaOH (10 M) than previous research on surface treatment of Ti (5 M) [17]. This

assumption is supported by our XPS spectra, which showed a low proportion of OH

groups on the treated metals with high Hf content in Fig. 1. It is reported that a lot of

$Na_2Ti_5O_{11}$ was mainly formed on Ti metal after 5 M-NaOH treatment and subsequent

heating at 600°C [17], while amount of $Na_2Ti_5O_{11}$ formed on the treated Ti-Hf alloy was

very low (See Fig. 2). Therefore, this may also lead to low apatite formation on the

present specimens in SBF. Chemical treatment of Hf metal with a more concentrated

NaOH solution might be necessary in future studies.

It is noted that the formed apatite contained $HPO_4^{2-}$ (See Fig. 4). Although Kokubo *et al.* developed bone-bonding Ti by 5 M-NaOH treatment and subsequent heat treatment at 600°C, the apatite layer formed in SBF has not been characterized by FT-IR. On the other hand, other groups have reported that $HPO_4^{2-}$-containing apatite is detected on Ti and its alloys treated with 10 M-NaOH and heated at 600°C after soaking in SBF [20,21]. Acidic dissociation of phosphoric acid is described as follows:

$$H_3PO_4 \rightleftharpoons H^+ + H_2PO_4^- \quad K_1 = 7.5 \times 10^{-3} \qquad (1)$$

$$H_2PO_4^- \rightleftharpoons H^+ + HPO_4^{2-} \quad K_2 = 6.2 \times 10^{-8} \qquad (2)$$

$$HPO_4^{2-} \rightleftharpoons H^+ + PO_4^{3-} \quad K_3 = 4.8 \times 10^{-13} \qquad (3)$$

It is assumed that approximately 60% of phosphate species takes a form of $HPO_4^{2-}$ at pH7.40 based on these equilibria. Therefore, ion exchange would occur between $HPO_4^{2-}$ in SBF and $CO_3^{2-}$ in the apatite crystals which are equivalent anion.

Apatite was not formed on the Ti-60Hf, with an intermediate composition. The proportion of OH groups on the surface of this substrate was similar to those of Ti-80Hf and pure Hf, which both promoted apatite formation (See Fig. 1). Therefore, the low proportion of OH groups was unlikely to be the reason for the lack of apatite formation.

12

Our zeta potential measurements indicated that the surface of $HfTiO_4$ was highly negatively charged (see Table 1). The surface charge was much lower than that of Ti metal subjected to the NaOH- and heat-treatments (approximately $-10$ mV), which formed apatite [22]. Apatite nucleation on negatively charged materials such as NaOH- and heat-treated Ti and Ta, and $Na_2O\text{-}SiO_2$ glass is triggered by initial $Ca^{2+}$ adsorption followed by $PO_4^{3-}$ adsorption [23,24,25]. Although Ca and P were detected on Ti-60Hf, the amounts were smaller than those of the other samples (see Fig. 3). Hence, we assume that the negative surface charge was neutralized by $Ca^{2+}$ adsorption onto $HfTiO_4$ but further $PO_4^{3-}$ adsorption was limited.

## 5. Conclusion

In this study, the apatite-forming abilities of pure Hf and Ti-Hf alloys subjected to NaOH- and heat-treatments were investigated in SBF. The following points were clarified.

(1) Pure Hf metal subjected to the treatments enabled formation of apatite on its surfaces. Therefore, Hf is a candidate metallic material, which exhibits bone-bonding potential.

(2) The apatite-forming ability of Ti-Hf alloys was low at intermediate compositions.

Namely, apatite formation was not observed in Ti-60Hf. We speculate that highly

negatively charged $HfTiO_4$ inhibited $PO_4^{3-}$ adsorption.

**References**

1.   Yamamoto A, Honma R, Sumita M. Cytotoxicity evaluation of 43 metal salts using

    murine fibroblasts and osteoblastic cells. J Biomed Mater Res 1998;39:331-340.

2.   Zhou YL, Niinomi M, Akahori T. Dynamic Young's Modulus and Mechanical

    Properties of Ti-Hf Alloys. Mater Trans 2004;45:1549-1554.

3.   Shiraishi T, Shishido T, Shinozaki N, Fujita T. The effects of Hf addition to Ti on

    its elastic modulus and corrosion resistance. J Jpn Soc Dent Mater Devices

2010;29:153 (in Japanese).

4. Wang BL, Li L, Zheng YF. In vitro cytotoxicity and emocompatibility studies of Ti-Nb,Ti-Nb-Zr and Ti-Nb-Hf biomedical shape memory alloys. Biomed Mater 2010;5:044102.

5. Kokubo T, Kim HM, Kawashita M. Novel bioactive materials with different mechanical properties. Biomaterials 2003;24:2161-2175.

6. Kim HM, Miyaji F, Kokubo T, Nakamura T. Preparation of bioactive Ti and its alloys via simple chemical surface treatment. J Biomed Mater Res 1996;32:409-417.

7. Wang XX, Hayakawa S, Tsuru K, Osaka A. A comparative study of in vitro apatite deposition on heat-, $H_2O_2$-, and NaOH-treated titanium surfaces. J Biomed Mater Res 2001;54:172-178.

8. Yang BC, Uchida M, Kim HM, Zhang X, Kokubo T. Preparation of bioactive titanium metal via anodic oxidation treatment. Biomaterials 2004;25:1003–1010.

9. Miyazaki T, Kim HM, Miyaji F, Kokubo T, Nakamura T. Bioactive Tantalum Metal Prepared by NaOH Treatment. J Biomed Mater Res 2000;50:35-42.

10. Uchida M, Kim HM, Miyaji F, Kokubo T, Nakamura T. Apatite formation on zirconium metal treated with aqueous NaOH. Biomaterials 2002;23:313-317.

11. Cho SB, Kokubo T, Nakanishi K, Soga N, Ohtsuki C, Nakamura T, Kitsugi T, Yamamuro T. Dependence of Apatite Formation on Silica Gel on Its Structure: Effect of Heat Treatment. J Am Ceram Soc 1995;78:1769-1774.

12. Nakao Y, Sugino A, Tsuru K, Uetsuki K, Shirosaki Y, Hayakawa S, Osaka A. Enhancement of apatite-forming ability of parallely aligned Ti-substrates with optimum gaps by autoclaving. J Ceram Soc Japan 2010;118:483-486.

13. Kokubo T, Ito S, Huang ZT, Hayashi T, Sakka S, Kitsugi T, Yamamuro T. Ca,P-rich layer formed on high-strength bioactive glass-ceramic A-W, J. Biomed. Mater. Res. 1990;24:331-343.

14. Kandori K, Horigami N, Yasukawa A, Ishikawa T. Texture and Formation Mechanism of Fibrous Calcium Hydroxyapatite Particles Prepared by Decomposition of Calcium–EDTA Chelates. J Am Ceram Soc 1997;80:1157–1164.

15. Drouet C. Apatite Formation: Why It May Not Work as Planned, and How to Conclusively Identify Apatite Compounds. Biomed Res Int 2013;2013:Article ID

490946.

16. Kim HM, Kishimoto K, Miyaji F, Kokubo T, Yao T, Suetsugu Y, Tanaka J, Nakamura T. Composition and structure of apatite formed on organic polymer in simulated body fluid with a high content of carbonate ion. J Mater Sci Mater Med 2000;11:421–426.

17. Kim HM, Miyaji F, Kokubo T, Nakamura T. Effect of Heat Treatment on Apatite-forming Ability of Ti Metal Induced by Alkali Treatment. J Mater Sci Mater Med 1997;8:341-347.

18. Corrosion Resistance of Titanium. TIMET Corporation Brochure Denver:1997:18.

19. Holmes DR. Corrosion of Hafnium and Hafnium Alloys. ASM Handbook, Volume 13B, Corrosion: Materials. OH:ASM International;2005:354-359.

20. Lin FH, Hsu YS, Lin SH, Chen TM. The growth of hydroxyapatite on alkaline treated Ti–6Al–4V soaking in higher temperature with concentrated $Ca^{2+}/HPO_4^{2-}$ simulated body fluid. Mater Chem Phys 2004;87:24-30.

21. Müller L, Müller FA. Preparation of SBF with different $HCO_3^-$ content and its influence on the composition of biomimetic apatites. Acta Biomater

2006;2:181-189.

22. Kim HM, Himeno T, Kawashita M, Lee JH, Kokubo T, Nakamura T. Surface

potential change in bioactive titanium metal during the process of apatite formation

in simulated body fluid. J Biomed Mater Res A. 2003;67:1305-1309.

23. Takadama H, Kim HM, Kokubo T, Nakamura T. An X-ray photoelectron

spectroscopy study of the process of apatite formation on bioactive titanium metal.

J Biomed Mater Res 2001;55:185-193.

24. Miyazaki T, Kim HM, Kokubo T, Ohtsuki C, Kato H, Nakamura T. Mechanism of

Bonelike Apatite Formation on Bioactive Tantalum Metal in Simulated Body Fluid.

Biomaterials 2002;23:827-832.

25. Takadama H, Kim HM, Kokubo T, Nakamura T. X-ray photoelectron spectroscopy

study on the process of apatite formation on a sodium silicate glass in simulated

body fluid. J Am Ceram Soc 2002;85:1933–1936.

18

Table 1　Zeta potentials of the samples (N=3)

| Sample | Zeta potential (mV) |
|---|---|
| $HfO_2$ | $-15.5 \pm 1.79$ |
| $HfTiO_4$ | $-41.9 \pm 2.05$* |

*$p < 0.001$ in comparison with $HfO_2$

**Figure captions**

**Fig. 1**  XPS spectra of NaOH- and heat-treated metal substrates. This shows that surface

OH content is different by composition of the alloy.

**Fig. 2**  TF-XRD patterns of NaOH- and heat-treated metal substrates before (left) and

after (right) immersion in SBF for 7 days. This shows that surface crystalline phase is

significantly different by composition of the alloy.

**Fig. 3**  SEM images and EDX spectra of NaOH- and heat-treated metal substrates after

immersion in SBF for 7 days. Star marks indicate the positions of EDX analysis. Apatite

formation was not observed for intermediate composition of Ti-60Hf.

**Fig. 4**  High-magnification SEM images and FT-IR ATR spectrum of the spherical

particles formed on the surface of the treated Ti-80Hf substrate after immersion in SBF

for 7 days. This shows that the formed apatite contains $HPO_4^{2-}$ and $CO_3^{2-}$.

1
2
3
4
5
6
7
8
9
10
11
12
13
14
15
16
17
18
19
20
21
22
23
24
25
26
27
28
29
30
31
32
33
34
35
36
37
38
39
40
41
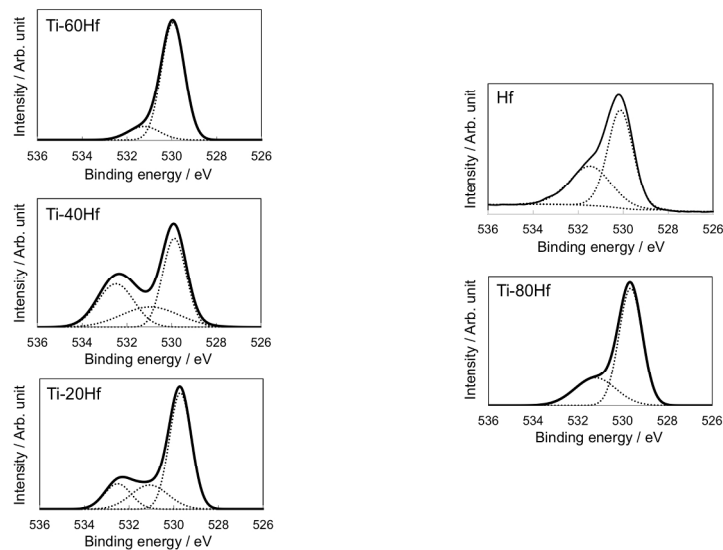42
43
44
45
46
47
48
49
50
51
52
53
54
55
56
57
58
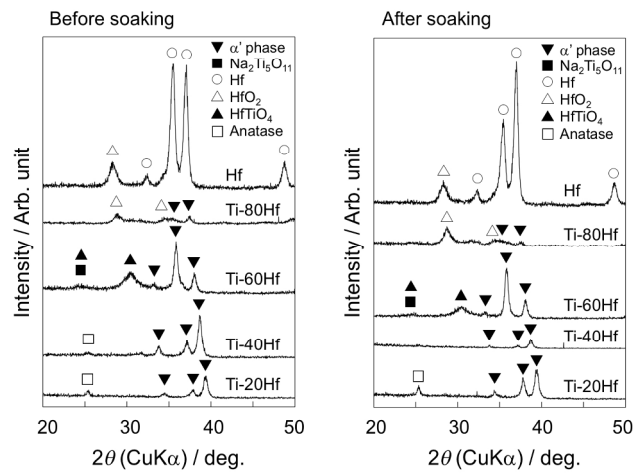59
60



Fig. 1

Fig.1

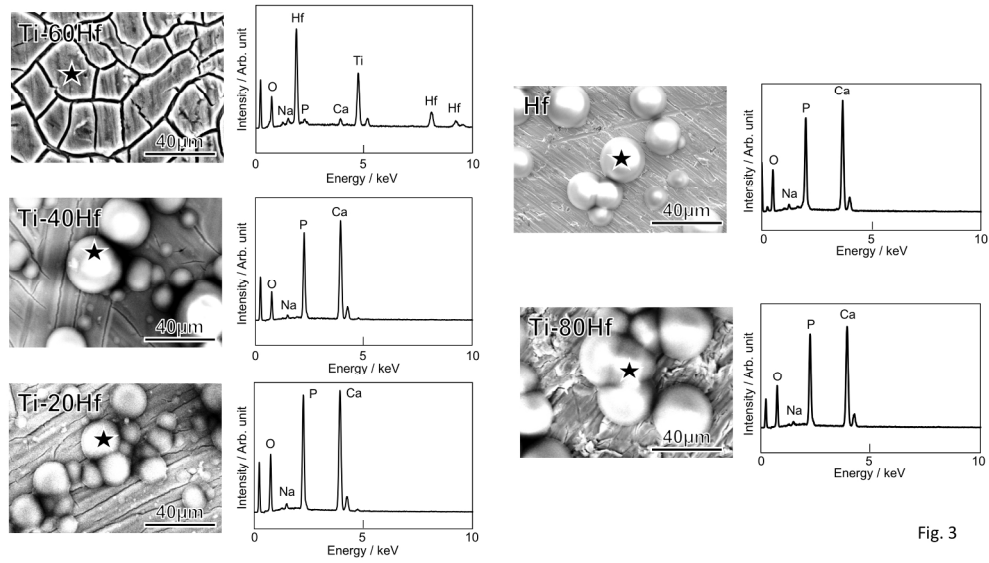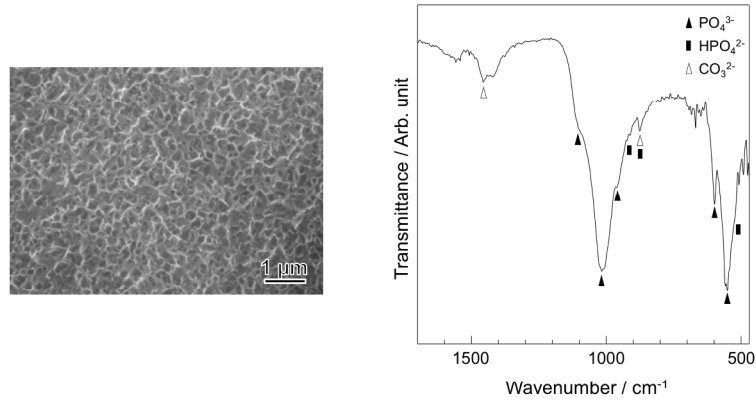338x190mm (180 x 180 DPI)

Fig.2

Fig.2

338x190mm (180 x 180 DPI)

Fig.3

338x190mm (180 x 180 DPI)

Fig. 4

Fig.4

338x190mm (180 x 180 DPI)